The Astrophysical Journal, 635:481–486, 2005 December 10

E_p-$E_{\rm iso}$ CORRELATION IN A MULTIPLE SUBJET MODEL OF GAMMA-RAY BURSTS

Kenji Toma,[1] Ryo Yamazaki,[2] and Takashi Nakamura[1]

Received 2005 April 28; accepted 2005 August 15

ABSTRACT

We perform Monte Carlo simulations to study the E_p-$E_{\rm iso}$ correlation in the context of a multiple-subjet model (or inhomogeneous jet model) for γ-ray bursts (GRBs), X-ray–rich GRBs (XRRs), and X-ray flashes (XRFs). For a single subjet, we find that $E_p \propto E_{\rm iso}^{0.4}$ for large viewing angles. For the multiple-subjet model in which all the subjets have the same intrinsic properties, off-axis events show $E_p \propto E_{\rm iso}^{a}$ with $0.4 < a < 0.5$. If the intrinsic properties of the subjets are distributed so that on-axis emission of each subjet follows a correlation $E_p \propto L_{\rm iso}^{1/2}$, we obtain the Amati correlation ($E_p \propto E_{\rm iso}^{1/2}$) over 3 orders of magnitude in E_p. Although the scatter around the Amati correlation is large in the simulation, the results are consistent with the observed properties of GRBs with known redshifts and the BASTE GRBs with pseudoredshifts derived from the lag-luminosity correlation. We also calculate the event rates, the redshift distributions, and the T_{90} duration distributions of GRBs, XRRs, and XRFs, which can be detected by *HETE-2*, assuming that the source redshift distribution is in proportion to the cosmic star formation rate. It is found that the event rates of the three classes are comparable, that the average redshift of the XRRs is a little larger than those of the GRBs and the XRFs, and that short XRRs arise when a single subjet is viewed off-axis or viewed on-axis with slightly high redshift.

Subject headings: gamma rays: bursts — gamma rays: theory

Online material: color figures

1. INTRODUCTION

HETE-2 (*High Energy Transient Explorer 2*) observations have provided strong evidence that softer and dimmer γ-ray bursts (GRBs) smoothly extend to X-ray flashes (XRFs) through an intermediate class of events called X-ray–rich GRBs (XRRs). For events with known redshifts and well-observed spectra, the rest-frame spectral peak energy E_p and the "bolometric" isotropic-equivalent γ-ray energy $E_{\rm iso}$ have a strong correlation, i.e., $E_p \propto E_{\rm iso}^{1/2}$ (Amati et al. 2002). This E_p-$E_{\rm iso}$ correlation, called the Amati correlation, has recently been extended down to lower energies characteristic of XRFs (Lamb et al. 2004). Since various observed quantities other than the Amati correlation also are distributed continuously among GRBs, XRRs, and XRFs (Sakamoto et al. 2005), it is strongly suggested that these three classes are related phenomena.

While many different models have been proposed for XRFs (see Granot et al. 2005 and references therein), we have proposed the "off-axis model" (Yamazaki et al. 2002, 2003) in which XRFs are the usual GRB jets viewed from an off-axis viewing angle (see also Woods & Loeb 1999). When the jet is observed off-axis, the emitted photons are out of the beaming cone and less blueshifted than photons emitted along the jet axis, so the events look like XRFs. It has been shown that the viewing angle of the jet is the key parameter for understanding the various properties of the GRBs and that the luminosity–variability/lag/width correlations might be naturally derived in the framework of off-axis models (Ioka & Nakamura 2001).

As for the Amati correlation, Yamazaki et al. (2004a) computed E_p and $E_{\rm iso}$ using the uniform jet model and found that the results are compatible with the observations. They also found that $E_p \propto E_{\rm iso}^{1/3}$ in the smaller $E_{\rm iso}$ regime. Eichler & Levinson (2004) investigated the correlation in an annular jet model and derived that if the viewing angles are within the annulus, $E_p \propto E_{\rm iso}^{a}$ with $\frac{1}{3} < a < \frac{1}{2}$, which is compatible with the observations. Compared with our uniform jet model, in the annular jet model the energy is large due to the emissions from widely distributed segments with similar viewing angles. Eichler & Levinson (2004) also anticipated that multiple discrete emissions could have the same effect.

The off-axis jet model has recently been improved to include short GRBs (Yamazaki et al. 2004b) as a unified model, according to which the GRB jet is not uniform but made up of multiple subjets or multiple emission patches. This is an extreme case of an inhomogeneous jet model (Nakamura 2000; Kumar & Piran 2000). The crucial parameter is the multiplicity, n_s, of the subjets along the line of sight. If $n_s \geq 2$, the burst looks like a long GRB; if $n_s = 1$, the burst looks like a short GRB; while if $n_s = 0$, the burst is an off-axis event for all the subjets and looks like an XRF or an XRR. We also found that the unified model may explain the bimodal distribution of the T_{90} durations of Burst and Transient Source Experiment (BATSE) GRBs (Toma et al. 2005).

In this paper, we examine the E_p-$E_{\rm iso}$ correlation in the multiple-subjet model to show that the unified model is consistent with the observations of E_p and $E_{\rm iso}$. This paper is organized as follows. In § 2, we describe our multiple-subjet model for prompt emissions. First, the E_p-$E_{\rm iso}$ correlation for a single subjet is discussed in § 3, and then we discuss the results of Monte Carlo simulations in the multiple-subjet model in § 4. Section 5 is devoted to discussion.

2. PROMPT EMISSION MODEL

Let us suppose that $N_{\rm tot}$ subjets with opening half-angle $\Delta\theta_{\rm sub}^{(j)}$ are launched from the central engine of a GRB randomly in time and directions and that the whole jet with opening half-angle $\Delta\theta_{\rm tot}$ consists of these subjets. We introduce the spherical

[1] Department of Physics, Kyoto University, Kyoto 606-8502, Japan; toma@tap.scphys.kyoto-u.ac.jp.

[2] Department of Earth and Space Science, Osaka University, Toyonaka 560-0043, Japan.

coordinate system (r, ϑ, φ) in the central engine frame, where the origin is the location of the central engine and $\vartheta = 0$ is the axis of the whole jet. The axis of the jth subjet ($j = 1, \cdots, N_{\rm tot}$) is denoted by $(\vartheta^{(j)}, \varphi^{(j)})$. If the direction of the observer is given by $(\vartheta_{\rm obs}, \varphi_{\rm obs})$, the viewing angle of the jth subjet from the line of sight is

$$\theta_v^{(j)} = \cos^{-1}[\sin\vartheta_{\rm obs}\sin\vartheta^{(j)}\cos(\varphi_{\rm obs}-\varphi^{(j)}) + \cos\vartheta_{\rm obs}\cos\vartheta^{(j)}]. \tag{1}$$

For the emission model of each subjet, we use the same formulations and notations as used in Yamazaki et al. (2003). Let us use another spherical coordinate system (r, θ, ϕ) in the central engine frame, where the origin is the location of the central engine and $\theta = 0$ is the line of sight. We adopt an instantaneous emission, at $t = t_0^{(j)}$ and $r = r_0^{(j)}$, of an infinitesimally thin shell moving with Lorentz factor $\gamma_{(j)}$. Then one can obtain the formula of the observed flux from the jth subjet with viewing angle $\theta_v^{(j)}$ at frequency ν and time T,

$$F_\nu^{(j)}(T) = \frac{2(1+z)r_0^{(j)}cA^{(j)}}{d_L^2}, \times \frac{\Delta\phi^{(j)}(T) f^{(j)}\left\{(1+z)\nu\gamma_{(j)}\left[1-\beta^{(j)}\cos\theta(T)\right]\right\}}{\gamma_{(j)}^2\left[1-\beta^{(j)}\cos\theta(T)\right]^2}, \tag{2}$$

where z and d_L are the redshift and the luminosity distance of the source, respectively; $f^{(j)}(\nu')$ and $A^{(j)}$ represent the spectral shape and the amplitude of the emission in the comoving frame, respectively. Here $T = 0$ is chosen as the time of arrival at the observer of a photon emitted at the origin at $t = 0$. The set of points that emit photons observed at a given time T is an arc (or a circle). The functions $\theta(T)$ and $\Delta\phi^{(j)}(T)$ represent an angular radius and a central angle of the arc, respectively:

$$\cos\theta(T) = \frac{c}{r_0^{(j)}}\left(t_0^{(j)} - \frac{T}{1+z}\right), \tag{3}$$

$$\Delta\phi^{(j)}(T) = \begin{cases} \pi, & \theta_v^{(j)} < \Delta\theta_{\rm sub}^{(j)} \text{ and } 0 < \theta(T) < \Delta\theta_{\rm sub}^{(j)} - \theta_v^{(j)}, \\ \cos^{-1}\left[\dfrac{\cos\Delta\theta_{\rm sub}^{(j)} - \cos\theta_v^{(j)}\cos\theta(T)}{\sin\theta_v^{(j)}\sin\theta(T)}\right], & \text{otherwise.} \end{cases} \tag{4}$$

Equation (3) can be rewritten by

$$1 - \beta^{(j)}\cos\theta(T) = \frac{1}{r_0^{(j)}/c\beta^{(j)}}\left(\frac{T}{1+z} - t_{\rm dep}^{(j)}\right), \tag{5}$$

where $t_{\rm dep}^{(j)} = t_0^{(j)} - r_0^{(j)}/c\beta^{(j)}$ is the departure time from the central engine of the jth subjet.

The observed spectrum of GRBs is well approximated by the Band spectrum (Band et al. 1993). In order to have a spectral shape similar to the Band spectrum, we adopt the following form of the spectrum in the comoving frame,

$$f^{(j)}(\nu') = \begin{cases} \left(\nu'/\nu_0'^{(j)}\right)^{1+\alpha_B^{(j)}} \times \exp\left(-\nu'/\nu_0'^{(j)}\right) & \text{for } \nu'/\nu_0'^{(j)} \le \alpha_B^{(j)} - \beta_B^{(j)}, \\ \left(\nu'/\nu_0'^{(j)}\right)^{1+\beta_B^{(j)}}\left(\alpha_B^{(j)} - \beta_B^{(j)}\right)^{\alpha_B^{(j)}-\beta_B^{(j)}} \times \exp\left(\beta_B^{(j)} - \alpha_B^{(j)}\right) & \text{for } \nu'/\nu_0'^{(j)} \ge \alpha_B^{(j)} - \beta_B^{(j)}, \end{cases} \tag{6}$$

where $\nu_0'^{(j)}$, $\alpha_B^{(j)}$, and $\beta_B^{(j)}$ are the break frequency and the low- and high-energy photon index, respectively.

As a summary, equations (2), (4), (5), and (6) are the basic equations for calculating the observed flux from each subjet, which depends on the following parameters: $\theta_v^{(j)}$ (which is determined by $\vartheta^{(j)}$, $\varphi^{(j)}$, $\vartheta^{\rm obs}$, and $\varphi^{\rm obs}$ through eq. [1]), $\Delta\theta_{\rm sub}^{(j)}$, $\gamma^{(j)}$, $t_{\rm dep}^{(j)}$, $r_0^{(j)}$, $\alpha_B^{(j)}$, $\beta_B^{(j)}$, $\nu_0'^{(j)}$, $A^{(j)}$, and z. The whole light curve from the GRB jet is produced by the superposition of the emissions from the subjets.

3. E_p-$E_{\rm iso}$ CORRELATION FOR A SINGLE SUBJET

Before examining the E_p-$E_{\rm iso}$ correlation for the multiple-subjet model, it is instructive to calculate the E_p-$E_{\rm iso}$ correlation when a single subjet is seen off-axis. Using equations (2), (4), (5), and (6) for $N_{\rm tot} = 1$ and a given θ_v, we compute the peak energy of the time-integrated spectrum measured in the cosmological rest frame, E_p, and the bolometric isotropic-equivalent energy, $E_{\rm iso}^s$, integrating over the 1–10^4 keV range in the cosmological rest frame. Here the superscript s of $E_{\rm iso}^s$ means "single." We adopt the following subjet parameters: $\Delta\theta_{\rm sub} = 0.02$ rad, $\gamma = 300$, $\alpha_B = -1$, $\beta_B = -2.5$, and $\gamma h\nu_0' = 350$ keV. In Figure 1, we show E_p and $E_{\rm iso}^s$ (in units of $2.8\times10^3\pi A r_0^2$) for 0 rad $< \theta_v <$ 0.1 rad (*solid line*). The dashed and dot-dashed lines are $(E_{\rm iso}^s)^{0.4}$ and $(E_{\rm iso}^s)^{1/3}$, respectively. We see that for $\theta_v > \Delta\theta_{\rm sub}$, as θ_v increases, both E_p and $E_{\rm iso}^s$ decrease. We focus on the small $E_{\rm iso}^s$ regime. At first, the E_p-$E_{\rm iso}$ correlation approaches $E_p \propto (E_{\rm iso}^s)^{0.4}$, but for even larger θ_v, $E_p \propto (E_{\rm iso}^s)^{1/3}$. This behavior is explained as follows. First, the spectral peak energy scales as $E_p \propto [1 - \beta\cos(\theta_v - \Delta\theta_{\rm sub})]^{-1}$ because of the Doppler effect, and for large θ_v, $E_p \propto \theta_v^{-2}$. Next, we compute $E_{\rm iso}^s$ by integrating equation (1) over ν and T and study its dependence on θ_v. When θ_v is large but E_p is in the 1–10^4 keV range, the integration over $\nu/(1+z)$ results in a constant depending on the Band spectral parameters and another Doppler factor $[1 - \beta\cos\theta(T)]^{-1}$. As for the integration with respect to T, we change the variable from T to $\theta(T)$ and obtain

$$E_{\rm iso}^s \propto \int_{\theta_v-\Delta\theta_{\rm sub}}^{\theta_v+\Delta\theta_{\rm sub}} \frac{\Delta\phi(\theta)\sin\theta\, d\theta}{(1-\beta\cos\theta)^3}. \tag{7}$$

For large θ_v, $\Delta\phi \simeq \Delta\theta_{\rm sub}/\theta_v$, so that $E_{\rm iso}^s \propto \theta_v^{-1}\{[1 - \beta\cos(\theta_v - \Delta\theta_{\rm sub})]^{-2} - [1 - \beta\cos(\theta_v + \Delta\theta_{\rm sub})]^{-2}\} \simeq \theta_v^{-1}[1 - \beta\cos(\theta_v - \Delta\theta_{\rm sub})]^{-2} \propto E_p^{2.5}$. When θ_v is even as large as $E_p \sim 1$ keV, the integration over $\nu/(1+z)$ results in a factor $(1 - \beta\cos\theta)^{1+\beta_B}$, so that the same calculation gives us $E_{\rm iso}^s \propto \theta_v^{-1}[1 - \beta\cos(\theta_v - \Delta\theta_{\rm sub})]^{\beta_B} \propto E_p^3$ for $\beta_B = -2.5$.

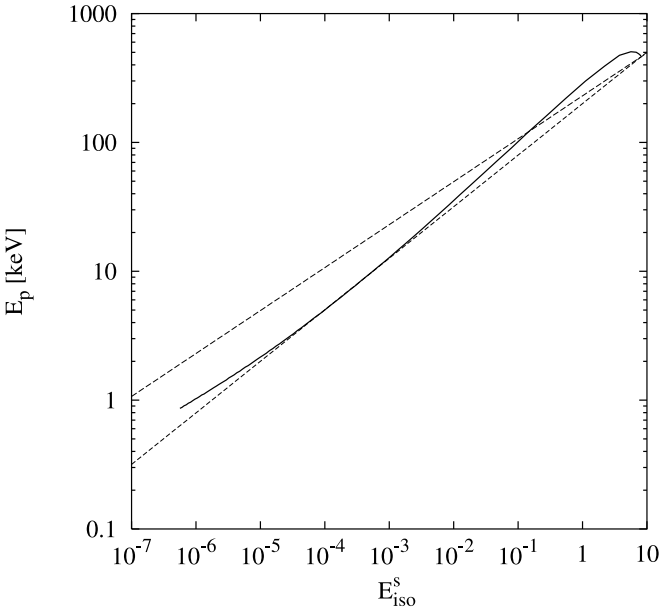

FIG. 1.—Correlation between isotropic-equivalent energy $E^s_{\rm iso}$ (in units of $2.8\times10^3\pi A r_0^2$) and spectral peak energy E_p for a single subjet; $(E^s_{\rm iso})^{0.4}$ (*dashed line*) and $(E^s_{\rm iso})^{1/3}$ (*dot-dashed line*) are also shown.

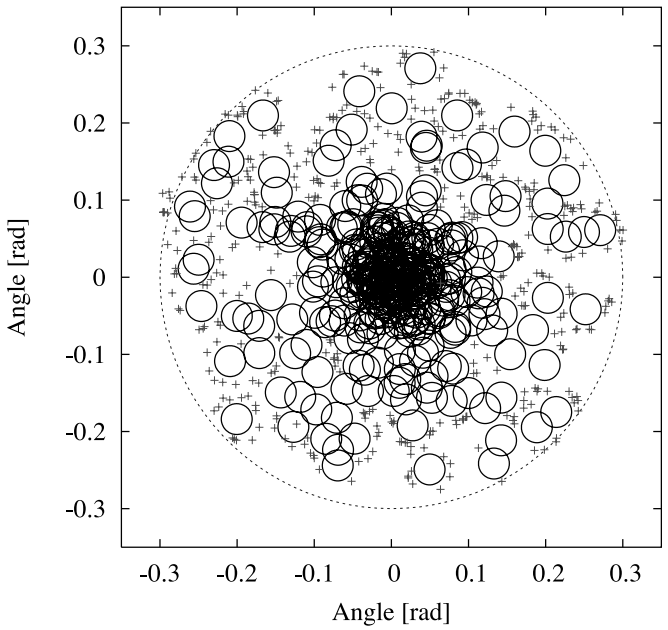

FIG. 2.—Angular distribution of $N_{\rm tot} = 350$ subjets confined in the whole GRB jet in our simulation. Each subjet is located according to the power-law distribution function of eq. (8). The whole jet has an opening half-angle of $\Delta\theta_{\rm tot} = 0.3$ rad. All subjets have equal opening half-angles of $\Delta\theta_{\rm sub} = 0.02$ rad. The angular size of the subjets is represented by the solid circles, while the whole jet is represented by the dashed circle. The viewing angles for detectable XRFs in our simulation are represented by plus signs. [*See the electronic edition of the Journal for a color version of this figure.*]

For a single subjet, off-axis events obey $E_p \propto E_{\rm iso}^{0.4}$ for the small E_p regime (but $E_p > 1$ keV). The index of the E_p-$E_{\rm iso}$ correlation, $a = 0.4$, is obtained irrespective of the intrinsic subjet parameters $\Delta\theta_{\rm sub}$, γ, $t_{\rm dep}$, r_0, α_B, β_B, ν_0', and A, as can be seen in the above derivation.

4. E_p-$E_{\rm iso}$ CORRELATION IN THE MULTIPLE-SUBJET MODEL

Let us perform Monte Carlo simulations to derive the E_p-$E_{\rm iso}$ correlation in the multiple-subjet model. For simplicity, we generate one GRB jet with opening half-angle $\Delta\theta_{\rm tot} = 0.3$ rad and 5000 random lines of sight to the observer with 0 rad $< \vartheta_{\rm obs} < 0.35$ rad according to the probability distribution of $\sin\vartheta_{\rm obs}\, d\vartheta_{\rm obs}\, d\varphi_{\rm obs}$. Then, for each observer, we calculate the peak energy of the time-integrated spectrum measured in the cosmological rest frame, E_p, and the bolometric isotropic-equivalent energy, $E_{\rm iso}$, integrating over the 1–10^4 keV range in the cosmological rest frame. The departure time of each subjet $t_{\rm dep}^{(j)}$ is assumed to be homogeneously random between $t = 0$ and $t = t_{\rm dur}$, where $t_{\rm dur}$ is the active time of the central engine measured in its own frame, and $t_{\rm dur} = 20$ s is adopted. The central engine is assumed to produce $N_{\rm tot} = 350$ subjets following the angular distribution function

$$\frac{dN}{d\Omega} \propto \begin{cases} 1, & 0 < \vartheta^{(j)} < \vartheta_c, \\ (\vartheta^{(j)}/\vartheta_c)^{-2}, & \vartheta_c < \vartheta^{(j)} < \vartheta_b, \end{cases} \tag{8}$$

where $\vartheta_b = \Delta\theta_{\rm tot} - \Delta\theta_{\rm sub}$ and $\vartheta_c = 0.03$ rad. This corresponds to the universal structured jet model (see Rossi et al. 2002; Zhang & Mészáros 2002a). The angular distribution of the subjets in our simulations is shown in Figure 2. The solid circles describe each subjet, and the dashed circle describes the whole jet. The meaning of the plus signs is discussed later. We assume that all of the subjets have the same values of the following parameters: $\Delta\theta_{\rm sub}^{(j)} = 0.02$ rad, $\gamma_{(j)} = 300$, $r_0^{(j)} = 3.0\times10^{14}$ cm, $\alpha_B^{(j)} = -1$, and $\beta_B^{(j)} = -2.5$. The intrinsic spectral parameter $\gamma h\nu_0'^{(j)}$ and the amplitude $A^{(j)}$ are determined so that the time-averaged emission from a single subjet viewed *on-axis* satisfies the correlation

$$\frac{L^s_{\rm iso}}{10^{52}\ {\rm ergs\ s^{-1}}} = \xi\left(\frac{E_p^s}{1\ {\rm keV}}\right)^2, \tag{9}$$

where $L^s_{\rm iso}$ is the time-averaged bolometric isotropic-equivalent luminosity and E_p^s is the time-averaged rest-frame spectral peak energy of the *on-axis* emission from a single subjet. As for the validity of this correlation, Liang et al. (2004) argue that for long bright BATSE GRBs the observed γ-ray flux F is correlated with the observed time-resolved $E_p^{\rm obs}$ at each time in a similar way, i.e., $F \propto (E_p^{\rm obs})^2$, which supports the assumption that the on-axis emission of each subjet obeys this correlation. Lloyd-Ronning & Ramirez-Ruiz (2002) show that there is a positive correlation between γ-ray luminosity and time-resolved rest-frame spectral peak energy by using variability-luminosity correlation (see also Yonetoku et al. 2004; Ghirlanda et al. 2005b). This correlation could be obtained by standard synchrotron internal shock model (e.g., Zhang & Mészáros 2002b). However, the coefficient ξ is highly uncertain. Therefore, we chose the values of ξ so that the results of simulations reproduce the observations. We consider two cases of $\gamma h\nu_0'^{(j)}$ and $A^{(j)}$: Case (*i*) $\gamma h\nu_0'^{(j)}$ and ξ are fixed as 350 keV and 6.0×10^{-5}, respectively, for all j. Case (*ii*) $\gamma h\nu_0'^{(j)}$ and ξ are distributed around the above values.

4.1. *Case (i)*

Let us consider case (*i*) as a simple toy model, in which all the subjets have the same intrinsic parameters, so that we can investigate the pure kinematical effects from the multiple discrete emission patches. The results are shown in Figure 3. The black solid line shows the E_p-$E_{\rm iso}$ correlation for a single subjet derived with the same parameters. We see that the black solid line

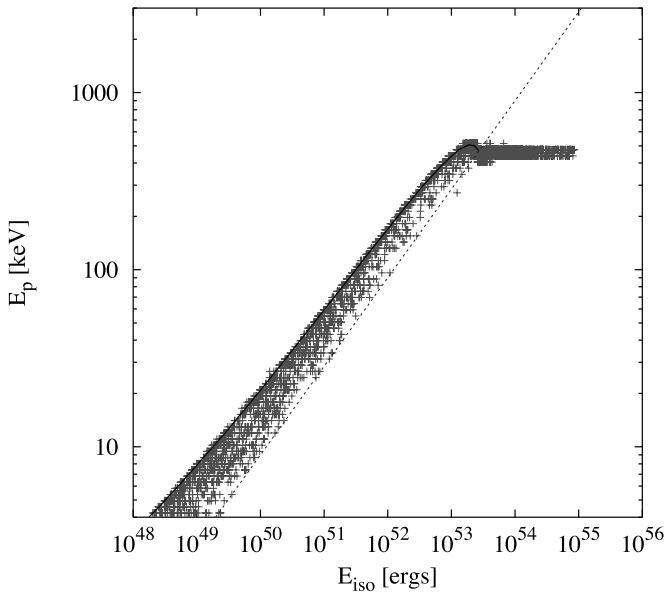

FIG. 3.—E_p-$E_{\rm iso}$ diagram in the multiple-subjet model in which all properties of each subjet are the same. The simulated bursts are represented by plus signs. The E_p-$E_{\rm iso}$ line for a single subjet is described by a solid line. The dashed line shows $E_p/1\ {\rm keV} = 90(E_{\rm iso}/10^{52}\ {\rm ergs})^{1/2}$. [*See the electronic edition of the Journal for a color version of this figure.*]

traces the left-hand edge of the distribution of the simulated bursts. When a single subjet is seen on-axis, the time-averaged spectral peak energy $E_p^s = g_n h\nu_0'/\gamma(1-\beta) \approx 2g_n\gamma h\nu_0' \sim 500\,{\rm keV}$, where a numerical factor $g_n(\sim 0.7)$ comes from the contribution of soft emission from the whole subjet, while $g_n = 1$ in the case of point-source approximation. The observed pulse has a duration determined by the angular spreading time as $\delta T = r_0\Delta\theta_{\rm sub}^2/2c = 2\,{\rm s}$. Then, according to equation (9), $L_{\rm iso}^s \simeq 1.5\times10^{53}$ ergs s^{-1}, so that $E_{\rm iso}^s = L_{\rm iso}^s\delta T \simeq 3\times10^{53}$ ergs. This corresponds to E_p reaching its maximum around $E_{\rm iso} \sim 3\times10^{53}$ ergs. When more than one subjet is seen on-axis, i.e., $n_s \geq 2$, E_p is the same as in the case of $n_s = 1$, but $E_{\rm iso} \simeq n_s E_{\rm iso}^s$. The maximum value of multiplicity n_s is about 30, when the line of sight is along the center of the whole jet. Then $E_{\rm iso}$ takes the maximum value of $\simeq 10^{55}$ ergs. Points with $E_p < 500$ keV correspond to the case of $n_s = 0$, in which all the subjets are seen off-axis; i.e., $\theta_v^{(j)} > \Delta\theta_{\rm sub}$ for all j. For each line of sight, the observed flux is dominated by the emission of the subjets with small $\theta_v^{(j)}$. Thus, E_p is determined by the minimum value of $\theta_v^{(j)}$, $\theta_v^{\rm min}$. Let $n_s^{\rm off}$ be the number of subjets with $\theta_v^{(j)}$ around $\theta_v^{\rm min}$. When $n_s^{\rm off} = 1$, the observed flux is dominated by a single subjet, and the $\theta_v^{\rm min}$-dependence of E_p and $E_{\rm iso}$ is determined as discussed in § 3. Such points are on the black solid line. When $n_s^{\rm off} \geq 2$, for each $\theta_v^{\rm min}$, E_p is the same as for the case of $n_s^{\rm off} = 1$, but $E_{\rm iso} \simeq n_s^{\rm off} E_{\rm iso}^s$. Thus, the scatter of the simulated points for $E_p < 500$ keV arises from that of $n_s^{\rm off}$. We find that the right-hand edge of the distribution of the points follows $E_p \propto E_{\rm iso}^{1/2}$. The reason for this behavior is as follows. For each $\theta_v^{\rm min}$, $E_p \propto [1-\beta\cos(\theta_v^{\rm min} - \Delta\theta_{\rm sub})]^{-1}$. The other quantity $E_{\rm iso}$ is given for the largest $n_s^{\rm off}$. Since the probability that these $n_s^{\rm off}$ subjets have the same axis $(\vartheta^{(j)}, \varphi^{(j)})$ is quite low, they should be smoothly distributed around the line of sight. Then in calculating $E_{\rm iso}$ by equation (7) for the multiple-subjet case, we can take $\Delta\phi \simeq \pi$. Therefore, for each $\theta_v^{\rm min}$, $E_{\rm iso} \propto [1-\beta\cos(\theta_v^{\rm min} - \Delta\theta_{\rm sub})]^{-2}$, and then we obtain $E_{\rm iso} \propto E_p^2$. Such a situation resembles the case of the annulus jet model in which the line of sight is inside the annulus and the inner radius of the annulus changes (see Eichler & Levinson 2004).

For a multiple-subjet model, off-axis events (with $n_s = 0$) follow $E_p \propto E_{\rm iso}^a$ with $0.4 < a < 0.5$. This range of a is obtained irrespective of the intrinsic subjet parameters $\Delta\theta_{\rm sub}$, γ, $t_{\rm dep}$, r_0, α_B, β_B, ν_0', and A.

4.2. *Case (ii)*

Here we assume that $\gamma h\nu_0'^{(j)}$ is distributed randomly according to a lognormal distribution function (Ioka & Nakamura 2002) with an average of log (350 keV) and a logarithmic variance of 0.2. For given $\gamma h\nu_0'^{(j)}$, $A^{(j)}$ is determined by equation (9). The coefficient ξ is also assumed to obey a lognormal distribution with an average of $-5 +$ log 6.0 and a logarithmic variance of 0.15. The other parameters of the subjets are fixed to the same values as in the previous simulation. We calculate $E_{\rm iso}$ and E_p and then assign a redshift for each observer to calculate the distance and the observed light curve. The source redshift distribution is assumed to be in proportion to the cosmic star formation rate. We adopt the model SF2 in Porciani & Madau (2001), in which we take the standard cosmological parameters of $H_0 = 70$ km s^{-1} Mpc^{-1}, $\Omega_M = 0.3$, and $\Omega_\Lambda = 0.7$. Finally, we select detectable events with observed peak photon fluxes in the 1–10^4 keV band larger than 1.0 photons cm^{-2} s^{-1}, which corresponds to the threshold sensitivity of *HETE-2* (see Band 2003; Lamb et al. 2005). Figure 4 shows the result of our simulation. Plus signs represent bursts that can be detected by *HETE-2*, while crosses represent those that cannot be detected. They are compared with the *BeppoSAX* and *HETE-2* data (*points with error bars*) taken from Ghirlanda et al. (2004). The solid line represents the best-fit line for 442 GRBs with redshifts estimated by the lag-luminosity correlation (Ghirlanda et al. 2005a). We see that our simulated GRBs cover the observed GRBs over 3 orders of E_p, so that our multiple-subjet model with the intrinsic correlation $E_p^s \propto (L_{\rm iso}^{s1/2})^{1/2}$ under the universal structured jet model is consistent with the observations.

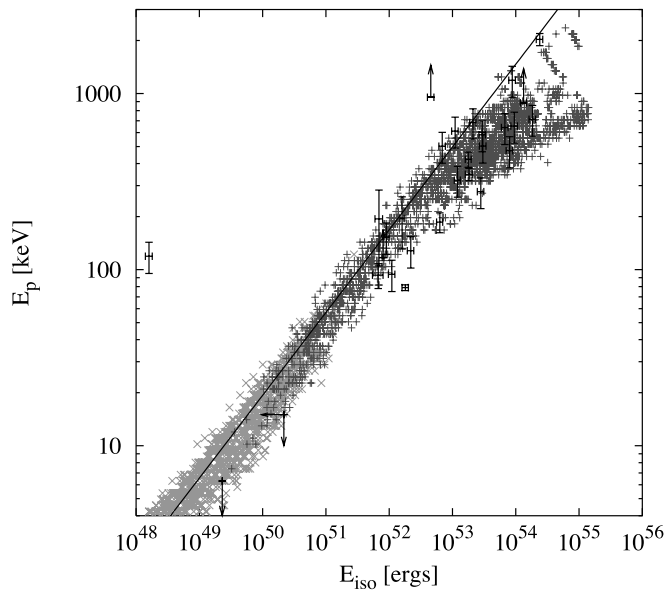

FIG. 4.—Same as Fig. 3, but in the multiple-subjet model in which subjet parameters $\gamma\nu_0'^{(j)}$, $A^{(j)}$, and ξ are distributed (see text for details). Plus signs represent bursts that can be detected by *HETE-2*, while crosses represent those that cannot be detected. They are compared with the *BeppoSAX* and *HETE-2* data (*points with error bars*) taken from Ghirlanda et al. (2004). The solid line represents the best-fit line for 442 GRBs with redshifts estimated by the lag-luminosity correlation (Ghirlanda et al. 2005a). [*See the electronic edition of the Journal for a color version of this figure.*]

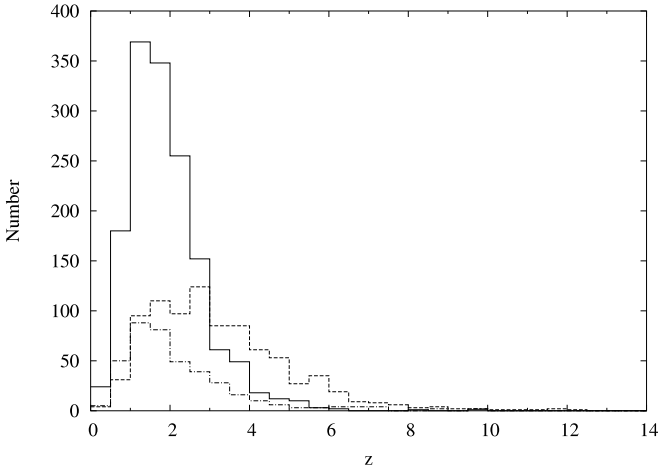

FIG. 5.—Redshift distribution of the simulated bursts surviving the peak photon flux truncation. The solid line, dashed line, and dot-dashed line represent the distribution for GRBs, XRRs, and XRFs, respectively.

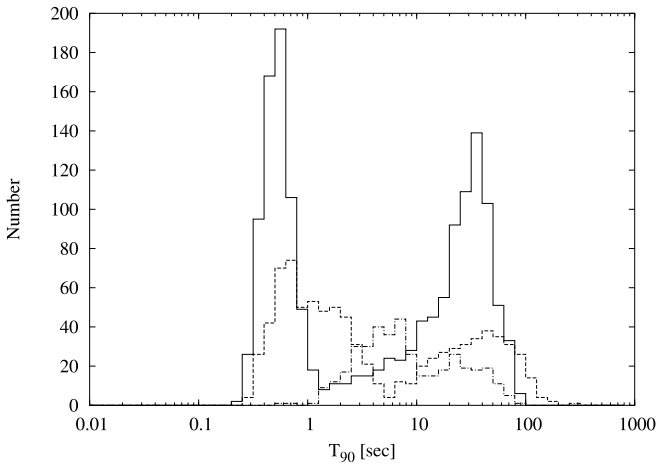

FIG. 6.—Distribution of the T_{90} durations in the 50–300 keV band of the simulated bursts surviving the peak flux truncation. Lines are as in Fig. 5.

The $n_s = 1$ bursts directly reflect the assumed correlation of $E_p^s \propto (L_{\rm iso}^s)^{1/2}$. For larger n_s, $E_{\rm iso}$ becomes larger, and E_p is determined by the subjet emission with the largest $L_{\rm iso}^s$ observed. As a result, all of the simulated bursts roughly obey $E_p \propto E_{\rm iso}^{1/2}$ over about 3 orders of magnitude in E_p. The scatter comes from the differences in the number of observed subjets and the differences in the parameters of each subjet.

5. DISCUSSION

We have investigated the E_p-$E_{\rm iso}$ correlation in a multiple-subjet model for GRBs, XRRs, and XRFs. We find that off-axis events (with $n_s = 0$) for multiple discrete emission regions show $E_p \propto E_{\rm iso}^a$ with $0.4 < a < 0.5$. It is assumed that the subjet parameters $\gamma h\nu_0'^{(j)}$ and $A^{(j)}$ are distributed so that the emission of the subjets viewed on-axis follows the correlation $E_p^s \propto (L_{\rm iso}^s)^{1/2}$, with a narrow E_p^s range (1 order of magnitude). Then the Amati correlation ($E_p \propto E_{\rm iso}^{1/2}$) is reproduced over 3 orders of magnitude in E_p. Although the scatter around the Amati correlation is large in the simulation, the results are consistent with the observed properties of GRBs with known redshifts and the BATSE GRBs with pseudoredshifts derived from the lag-luminosity correlation. We argue that for brighter bursts the Amati correlation arises from an intrinsic property, while for dimmer bursts it arises from the off-axis effects of multiple emissions. The intrinsic $E_p^s \propto (L_{\rm iso}^s)^{1/2}$ correlation is supported by the observations (Liang et al. 2004; Lloyd-Ronning & Ramirez-Ruiz 2002) and could be derived in the context of the standard synchrotron internal shock model.

The *HETE* team defines XRRs and XRFs as those events for which $\log [S_X(2-30\ {\rm keV})/S_\gamma(30-400\ {\rm keV})] > -0.5$ and 0.0, respectively (Lamb et al. 2004). We calculate the observed fluence ratio for simulated bursts surviving the peak flux truncation and classify them into GRBs, XRRs, and XRFs. The ratio of the simulated event rates is $R_{\rm GRB}:R_{\rm XRR}:R_{\rm XRF} \sim 4:3:1$. *HETE-2* observations show a similar number of GRBs, XRRs, and XRFs (Sakamoto et al. 2005). We can say that the event rate among GRBs, XRRs, and XRFs is consistent with the observations. Figure 5 shows the redshift distribution of GRBs (*solid line*), XRRs (*dashed line*), and XRFs (*dot-dashed line*). The mean redshifts of GRBs, XRRs, and XRFs are 1.9, 3.2, and 2.3, respectively. XRRs have slightly larger redshifts than GRBs and XRFs. Figure 2 plots the viewing angles for detectable XRFs, which are represented by plus signs. We see that the main population of XRFs arises from the off-axis effects. On the other hand, many XRRs are on-axis events. Since $E_p > 200$ keV for on-axis events in our simulation, the on-axis XRRs arise from the cosmological redshift effect. The ratio of the on-axis and off-axis XRRs is $\sim 1:1$. We expect the event rate ratio from larger observed samples to give us some information about the angular distribution of the subjets within the whole GRB jet and the redshift distribution of the GRB sources.

In this paper, we have performed the simulations with a fixed Lorentz factor of the subjets, $\gamma = 300$. As discussed in § 4, the range of the index a of the E_p-$E_{\rm iso}$ correlation for off-axis events is independent of the Lorentz factor. We perform the same simulations in case (*ii*) for $\gamma = 100$ and 500 and obtain the Amati correlation ($E_p \propto E_{\rm iso}^{1/2}$) through all bursts. However, the peak photon flux of the XRFs is small for lower Lorentz factor. For $\gamma = 100$, we obtain $R_{\rm GRB}:R_{\rm XRR}:R_{\rm XRF} \sim 15:10:1$. Alternatively, for $\gamma = 500$, $R_{\rm GRB}:R_{\rm XRR}:R_{\rm XRF} \sim 3:2:1$.

Figure 6 shows the distribution of the T_{90} durations in the 50–300 keV band for GRBs (*solid line*), XRRs (*dashed line*), and XRFs (*dot-dashed line*). GRBs have a bimodal distribution as observed by BATSE. We have already shown why GRBs have the bimodal duration distribution in our multiple-subjet model (Toma et al. 2005): the T_{90} duration of an $n_s = 1$ burst is determined by the width of a single pulse, while that of an $n_s \geq 2$ burst is determined by the time interval between the observed first pulse and the last one. These two different timescales naturally lead to a division of the burst T_{90} durations into short and long ones. We also calculate the distribution of the T_{90} durations in the 2–25 keV band. Figure 7 shows the result. These distributions are not inconsistent with the *HETE-2* data (see Fig. 4 of Sakamoto et al. 2005). The T_{90} durations of $n_s = 1$ bursts (i.e., short bursts) become larger when they are measured in the softer band, since soft emission from the periphery of the subjet is observed for a longer time. Yamazaki et al. (2004b) have predicted short XRRs in our unified model, which are confirmed in this simulation. These are events of a single subjet viewed off-axis or viewed on-axis with slightly high redshift. Indeed, GRB 040924 may be an example of a short XRR, from which recent *Hubble Space Telescope* (*HST*) observation reveals a supernova signature (Soderberg et al. 2005). This event supports our unified picture.

In this paper, we have considered the θ^{-2}-angular distribution of the subjets. Averaging by a solid angle satisfying $(\Delta\theta_{\rm sub})^2 < \Omega < (\Delta\theta_{\rm tot})^2$, the distribution of the emission energy (or, almost equivalently, the angle-averaged kinetic energy) is the same as that of the universal structured jet model (Rossi et al. 2002; Zhang & Mészáros 2002a). The universal structured jet model

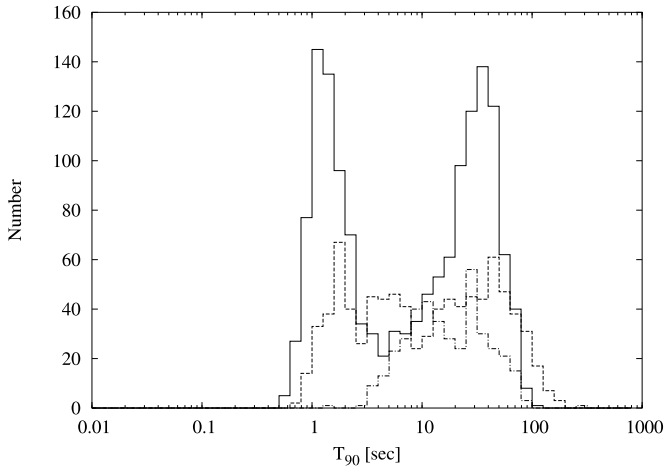

FIG. 7.—Same as Fig. 6, but for the 2–25 keV band.

was criticized by Lamb et al. (2005): in the universal structured jet model, it is assumed that XRFs are observed when the jet is viewed from a fairly large angle, so that the model overpredicts the number of XRFs, which is inconsistent with the observed ratio of the number of XRFs and GRBs detected by *HETE-2*. Then, Zhang et al. (2004) modified the universal structured jet model and showed that if the jet is structured with a Gaussian-like shape, the number of XRFs becomes small. In these works it is assumed that the jet is continuous and there are no cold spots inside the jet. As shown in this paper, Eichler & Levinson (2004), and Yamazaki et al. (2004b), if the observer points toward a cold spot (i.e., $n_s = 0$), XRFs or XRRs are observed; while if $n_s \geq 2$, the event looks like a long GRB irrespective of the viewing angle. In our model, the ratio of the total solid angle with $n_s \geq 2$ and $n_s = 0$ determines the event rate of GRBs and XRRs/XRFs. Interestingly, we find that a power-law profile with an index of -2 is preferable to a Gaussian profile in order to reproduce the ratio of the observed event rate of GRBs, XRRs, and XRFs because the solid angle with $n_s = 0$ is small in the Gaussian profile. Lazzati & Begelman (2005) have recently argued that in the context of the collapsar model, a θ^{-2} angular profile might be obtained as a consequence of the physics in the jet breakout irrespective of the jet structure inside the progenitor. From the observational side, we can estimate the pseudo–jet opening angle distribution. Using the Ghirlanda correlation ($E_p \propto E_\gamma^{0.71}$), where $E_\gamma = E_{\rm iso}\theta_j^2/2$ (Ghirlanda et al. 2004), and the Yonetoku correlation ($E_p \propto L_p^{0.5}$), where L_p is a peak luminosity (Yonetoku et al. 2004), Yonetoku et al. (2005) obtained that the pseudo–jet opening angle obeys $f(\theta_j)d\theta_j \propto \theta_j^{-2}d\theta_j$. This is compatible with the power-law structured jet model: if all bursts were observable, the distribution would be uniform per unit solid angle and $f(\theta) \propto \theta$. However, $E_{\rm iso}$ for the smaller viewing angle is brighter by a factor of θ^{-2}, so that the maximum observable distance is larger by a factor of θ^{-1}, which contains a volume larger by a factor of θ^{-3}. Then we have $f(\theta) \propto \theta^{-2}$.

The late-phase evolution of a set of multiple subjets is rather complicated and hard to predict. Cold spots do not produce high-energy emission but may be filled with kinetic energy that is not dissipated at small radius (see also Levinson & Eichler 2005). Even if cold spots are not filled with kinetic energy, all subjets begin to expand sideways and would merge into one shell. In any case, late afterglow behavior may be well approximated by the results from the continuous structured jet model (e.g., Kumar & Granot 2003). As shown in Figure 2, almost all XRFs arise when all the subjets are viewed off-axis, i.e., $n_s = 0$, while the observers see the whole jet on-axis. Then, the late-phase ($\gtrsim$1 day) properties of XRF afterglows may not be like orphan afterglows but may show similar behavior to those of normal GRBs (e.g., Amati et al. 2004). On the other hand, as rare cases, when the whole jet is viewed off-axis, XRF afterglows may resemble the orphan afterglow (e.g., Granot et al. 2005). XRF 030723 may be a member of such a class (Butler et al. 2005; Fynbo et al. 2004).

We are grateful to the referee for useful comments. K. T. thanks M. Ohashi for helpful discussions. This work is supported in part by a Grant-in-Aid for the 21st Century COE "Center for Diversity and Universality in Physics" from the Ministry of Education, Culture, Sports, Science, and Technology (MEXT) of Japan and also by Grants-in-Aid for Scientific Research of the Japanese Ministry of Education, Culture, Sports, Science, and Technology 09245 (R. Y.), 14047212 (T. N.), 14204024 (T. N.), and 17340075 (T. N.).

REFERENCES

Amati, L., et al. 2002, A&A, 390, 81
———. 2004, A&A, 426, 415
Band, D. L. 2003, ApJ, 588, 945
Band, D. L., et al. 1993, ApJ, 413, 281
Butler, N. R., et al. 2005, ApJ, 621, 884
Eichler, D., & Levinson, A. 2004, ApJ, 614, L13
Fynbo, J. P. U., et al. 2004, ApJ, 609, 962
Ghirlanda, G., Ghisellini, G., & Firmani, C. 2005a, MNRAS, 361, L10
Ghirlanda, G., Ghisellini, G., Firmani, C., Celloti, A., & Bosnjak, Z. 2005b, MNRAS, 360, L45
Ghirlanda, G., Ghisellini, G., & Lazzati, D. 2004, ApJ, 616, 331
Granot, J., Ramirez-Ruiz, E., & Perna, R. 2005, ApJ, 630, 1003
Ioka, K., & Nakamura, T. 2001, ApJ, 554, L163
———. 2002, ApJ, 570, L21
Kumar, P., & Granot, J. 2003, ApJ, 591, 1075
Kumar, P., & Piran, T. 2000, ApJ, 535, 152
Lamb, D. Q., Donaghy, T. Q., & Graziani, C. 2005, ApJ, 620, 355
Lamb, D. Q., et al. 2004, NewA Rev., 48, 423
Lazzati, D., & Begelman, M. C. 2005, ApJ, 629, 903
Levinson, A., & Eichler, D. 2005, ApJ, 629, L13
Liang, E. W., Dai, Z. G., & Wu, X. F. 2004, ApJ, 606, L29
Lloyd-Ronning, N. M., & Ramirez-Ruiz, E. 2002, ApJ, 576, 101
Nakamura, T. 2000, ApJ, 534, L159
Porciani, C., & Madau, P. 2001, ApJ, 548, 522
Rossi, E., Lazzati, D., & Rees, M. J. 2002, MNRAS, 332, 945
Sakamoto, T., et al. 2005, ApJ, 629, 311
Soderberg, A. M., et al. 2005, ApJ, submitted (astro-ph/0504359)
Toma, K., Yamazaki, R., & Nakamura, T. 2005, ApJ, 620, 835
Woods, E., & Loeb, A. 1999, ApJ, 523, 187
Yamazaki, R., Ioka, K., & Nakamura, T. 2002, ApJ, 571, L31
———. 2003, ApJ, 593, 941
———. 2004a, ApJ, 606, L33
———. 2004b, ApJ, 607, L103
Yonetoku, D., Murakami, T., Nakamura, T., Yamazaki, R., Inoue, A. K., & Ioka, K. 2004, ApJ, 609, 935
Yonetoku, D., Yamazaki, R., Nakamura, T., & Murakami, T. 2005, MNRAS, 362, 1114
Zhang, B., Dai, X., Lloyd-Ronning, N. M., & Mészáros, P. 2004, ApJ, 601, L119
Zhang, B., & Mészáros, P. 2002a, ApJ, 571, 876
———. 2002b, ApJ, 581, 1236